

Origin of Stereoinduction by Chiral Aminophosphane Phosphinite Ligands in Enantioselective Catalysis: Asymmetric Hydroformylation

Jorge J. Carbó,^{*[a, b]} Agustí Lledós,^[c] Dieter Vogt,^[d] and Carles Bo^{*[a, b]}

Abstract: The origin of stereoinduction by chiral aminophosphane phosphinite (AMPP) ligands in asymmetric hydroformylation was investigated with a theoretical approach. The roles of the stereogenic center at the aminophosphane phosphorus atom (NP*) and of the chirality of the backbone were analyzed by considering three experimentally tested cases: 1) P-stereogenic yielding high *ee*, 2) P-nonstereogenic yielding low *ee*, and 3) P-stereogenic yielding low *ee*. We succeeded in reproducing the experimentally observed trends for the three studied AMPP ligands. Our results indicated that

alkene insertion into the rhodium–hydride bond is the selectivity-determining step, and not alkene coordination. Additional calculations on model systems revealed that the different non-bonding weak-type interactions of styrene with the substituents of the NP* stereogenic center in an axial position is responsible for stereodifferentiation. The chirality of the AMPP backbone

plays a secondary role. The rationalization of the stereochemical outcome is not straightforward, because two competitive equatorial/axial reaction paths, showing opposite asymmetric induction, must be considered. Construction of stereochemical models and evaluation of stereoinduction for novel ligand systems suggested that two prerequisites are required to improve the performance of AMPP-type ligands in asymmetric hydroformylation: 1) combination of stereorecognition and steric hindrance by substituents at the NP* atom, and 2) more rigid backbones.

Keywords: asymmetric catalysis • density functional calculations • hybrid QM/MM calculations • hydroformylation • P ligands

Introduction

Nowadays, there is enormous interest in obtaining enantiomerically pure compounds as building blocks for pharmaceuticals and bioactive agents. Homogeneous asymmetric catalysis is becoming one of the most successful tools to obtain chiral compounds from cheap substrates.^[1] In the last few years, asymmetric hydroformylation has attracted much interest as a potential tool for preparing enantiomerically pure aldehydes.^[2] A real breakthrough occurred in this field with the discovery of the Rh/BINAPHOS catalysts by Takaya et al.^[3] Since then new active chiral ligands such as diphosphites,^[4] phosphane phosphoramidites,^[5] aminophosphane phosphinites,^[6] and others^[7] have been developed. However, hydroformylation has yet not been of frequent use in organic synthesis.^[2] The most difficult problem with these processes is simultaneous control of enantio- and regioselectivity.


The chiral aminophosphane phosphinite (AMPP) ligand family was synthesized and successfully applied in enantioselective hydrogenation in the 1980.^[8] Since then, many other syntheses and applications of AMPP and closely related ligands have been reported.^[6,9–10] Recently, new chiral AMPP

[a] Dr. J. J. Carbó, Dr. C. Bo
Departament de Química Física i Inorgànica
Universitat Rovira i Virgili, Campus Sescelades
Marcel·lí Domingo s/n, 43007 Tarragona (Spain)
Fax: (+34) 977-559-563
E-mail: j.carbo@urv.net
cbo@iciq.es

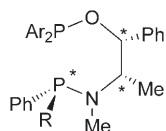
[b] Dr. J. J. Carbó, Dr. C. Bo
Institute of Chemical Research of Catalonia (ICIQ)
43007 Tarragona (Spain)

[c] Prof. A. Lledós
Unitat de Química Física, Edifici Cn
Universitat Autònoma de Barcelona
08193 Bellaterra (Spain)

[d] Prof. Dr. D. Vogt
Schuit Institute of Catalysis
Laboratory of Homogeneous Catalysis
Eindhoven University of Technology
P.O. Box 513, 56000 MB Eindhoven (The Netherlands)

 Supporting information for this article is available on the WWW under <http://www.chemeurj.org/> or from the author.

ligands, with a stereogenic center at the P(N) atom, were developed.^[6] Their application in rhodium-catalyzed asymmetric hydroformylations of vinyl arenes reached high enantiomeric excess. Although the BINAPHOS ligand remains a benchmark in asymmetric hydroformylation, the AMPP ligand family provides enormous potential for variation and ligand fine-tuning for a number of transition metal catalyzed reactions.^[9] Vogt et al. have



Scheme 1.

varied the substituents at the P(N) and at P(O) centers to study their influence on enantioselectivity (Scheme 1, Table 1).^[6] The results highlight that the presence of the addi-

Table 1. Selected results from reference [6] for aminophosphane phosphinite ligands (L) and hydroformylation of styrene with [HRh(L)(CO)₂] (L = a–i). See Scheme 1 for definitions of R and Ar.

Ligand	R	Ar	ee [%]
a	CH ₃	Ph	75
b	CH ₃	4-CH ₃ -C ₆ H ₄	71
c	CH ₃	3,5-(CF ₃) ₂ -C ₆ H ₃	32
e	<i>n</i> Bu	Ph	75
g	<i>n</i> Bu	3,5-(CF ₃) ₂ -C ₆ H ₃	46
h	Ph	Ph	10
i	1-naphthyl	Ph	10

tional stereogenic aminophosphane phosphorus atom seems to be crucial for obtaining good enantioselectivities. Note that in ligand **h** (R = Ph) without a stereogenic center at the phosphorus atom, the enantioselectivity drops considerably as compared to ligand **a** (R = CH₃). On the other hand, the introduction of a 1-naphthyl group (ligand **i**) also resulted in a decrease in enantioselectivity, despite the presence of a P(N) stereogenic center. Moreover, in situ NMR and IR studies of hydrido rhodium complexes under syngas pressure revealed that the ligand coordination mode also has a great influence in controlling enantioselectivity. Ligands that give high *ee* coordinate in a stable axial/equatorial manner, with the aminophosphane moiety in the axial position of the trigonal-bipyramidal complex.

Despite the rapid evolution of asymmetric catalysis, progress in catalyst development is often guided by trial-and-error approaches rather than by rational design. There is a lack of a fundamental understanding of when and how enantioselectivity is controlled. In many cases the enantioselectivity of a reaction is lower than the inherent selectivity of a catalyst because of an unselective background reaction, catalytically active impurities, or partial dissociation of a chiral ligand. Theoretical methods allow these kinds of problems to be avoided by determining the catalyst's ability for enantiodiscrimination by directly examining the catalyst–reactant complex rather than by experimental product analysis. Several theoretical studies on hydroformylation have been published lately, especially DFT and hybrid quantum mechanics/molecular mechanics (QM/MM) methods. These studies in-

clude cobalt, unmodified rhodium, and phosphane-modified rhodium catalysts. Most of the work has been reviewed,^[11–13] but several aspects of hydroformylation are still under investigation.^[14–18,22–24] The entire catalytic cycle for rhodium/phosphane-catalyzed hydroformylation has been examined at different levels of calculation by using simplified model phosphanes and ethene as model alkene.^[14–16] Recently, Rocha and Almeida used propene instead of ethene as substrate to investigate the regioselectivity on HRh(CO)(PH₃)₂ model rhodium/phosphane catalysts,^[17a] and on HRh(CO)₃ unmodified rhodium catalysts.^[17b] Alagona et al. also studied the regioselectivity for reaction of several vinyl substrates with unmodified rhodium catalysts.^[18] Nowadays, the main research interest in homogenous catalysis is focused on the development of new ligands with tailored stereoelectronic properties. The development of QM/MM methods such as IMOMM^[19] and the derived ONIOM method^[20] has enabled the investigation of real-size phosphane ligands.^[21–24] Also, previous theoretical approaches were performed using exclusively MM methods^[25] and semiquantitative “QM then MM” methods.^[26,27] Until now most of the effort has been devoted to the regioselectivity issue,^[17,18,21–26] whereas only few studies have been reported on the nature of enantioselectivity.^[27] Herrmann et al. made a first contribution to the theoretical description of asymmetric hydroformylation for BINAPHOS^[27a] and a series of C₂-symmetric bis-phosphane ligands.^[27b] They used a combined “QM then MM” approach, which has some limitations due to the lack of relaxation of reactive centers (in the QM region) under the influence of the ligands. Nevertheless, they succeeded in proposing a molecular model to explain the observed stereoselectivity for BINAPHOS.

The promising results of AMPP ligands in asymmetric hydroformylation, along with our previous analysis of hydroformylation regioselectivity,^[11,21] prompted us to perform a theoretical study on experimentally tested AMPP systems. We made use of first-principles quantum mechanics/molecular mechanics (QM/MM) based on the IMOMM scheme and pure quantum mechanics on the [HRh(CO)(AMPP)-(styrene)] real-world system. Our goal is to provide a quantitative theoretical characterization of the stereochemical outcome of a hydroformylation reaction with chiral AMPP ligand systems and their derivatives, and to explain the particular role of the P-stereogenic center. We selected three ligand systems **a**, **h**, and **i**, which represent respectively the three cases of P-stereogenic yielding high *ee*, P-nonstereogenic yielding low *ee*, and P-stereogenic yielding low *ee* (see Table 1). The substrate of choice is styrene, a common model substrate in asymmetric hydroformylation. In addition, we theoretically evaluated the stereochemical performance of novel target ligand systems. Furthermore, this study aims to gain insight into the origin of enantioselectivity in asymmetric hydroformylation with bidentate phosphane ligands, and if possible, to direct experimentalists towards the synthesis of novel efficient catalyst systems.

Computational Details

DFT calculations were carried out using the Amsterdam density functional program (ADFv2000) developed by Baerends et al.^[28] The electronic configurations of the molecular systems were described by a triple- ζ plus polarization Slater-type basis set, as included in the ADF package (Basis set IV), on the rhodium atom. Double- ζ plus polarization Slater-type basis set (Basis set III) were used for phosphorus, oxygen, carbon, nitrogen, and hydrogen atoms. The 1s–3d electrons for Rh, the 1s electrons for C, O, and N, and the 2p electrons for P were treated as frozen cores. Energies and geometries were evaluated by augmenting the local VWN exchange-correlation potential with Becke's nonlocal exchange-correlation correction^[29] and Perdew's correlation corrections^[30] (BP86). Quasirelativistic corrections were used for the core electrons alongside the Pauli formalism with corrected core potentials. The quasirelativistic frozen core shells were generated with the auxiliary program DIRAC^[28] included in the ADFv2000 package.

For the hybrid QM/MM calculations, we applied the IMOMM method^[19] as implemented in the ADF package.^[31] The QM region of the catalysts included the aminophosphane phosphinite backbone $\text{RhH}(\text{CO})(\text{H}_2\text{POCH}_2\text{CH}_2\text{NHPH}_2)$, while the substrate, ethene or styrene, was C_2H_2 . The molecular QM/MM partition is represented in Scheme 2. The QM level was the same as mentioned above. SYBYL force field^[32] was used as implemented in ADF to describe the atoms included in the MM part. The van der Waals parameters for the rhodium atom were taken from the UFF force field,^[33] and torsional contributions involving dihedral angles with the metal atom in terminal position were set to zero. The ratio between the P–C(aromatic) bond and the P–H bond lengths was 1.287, between C(sp²)–C(aromatic) and C(sp²)–H 1.387, between P–C(sp³) and P–H 1.289, between C(sp³)–C(aromatic) and C(sp³)–H 1.386, between C(sp³)–C(sp³) and C(sp³)–H 1.400, and between N–C(sp³) and N–H 1.361.

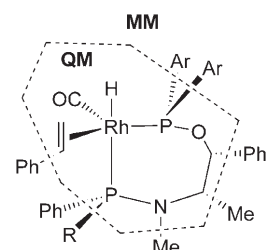
The minima were localized by full optimization of the starting structures. Transition states were initially localized for the model system $\text{RhH}(\text{CO})(\text{H}_2\text{POCH}_2\text{CH}_2\text{NHPH}_2)(\text{ethene})$. Convergence criteria in transition state search were set to 2×10^{-3} a.u. on the maximum Cartesian gradient, and to 2×10^{-4} a.u. on the energy. Vibrational frequency analysis was performed by double numerical differential of the energy gradients on the four possible isomers (see below). Transition states were characterized by single imaginary frequency, except for the case of the phosphinite-rotation side at position I (see Figure 3 and next section for details), in which a small residual negative frequency (-10.3 cm^{-1}) was found. Attempts to get rid of the residual negative frequency were unsuccessful. However, in all cases the normal mode of the largest imaginary frequency corresponded to the expected motion. In the case of QM/MM calculations, for which vibrational frequencies are not available, transition state searches were started from the characterized geometries of the model system. First, the reaction-center coordinates (rhodium, hydride, and olefinic carbon atoms) were kept fixed while all the other degrees of freedom were fully optimized. Then transition state searches were performed by making use of the Hessians describing the expected shapes of the potential energy hypersurface.

Results and Discussion

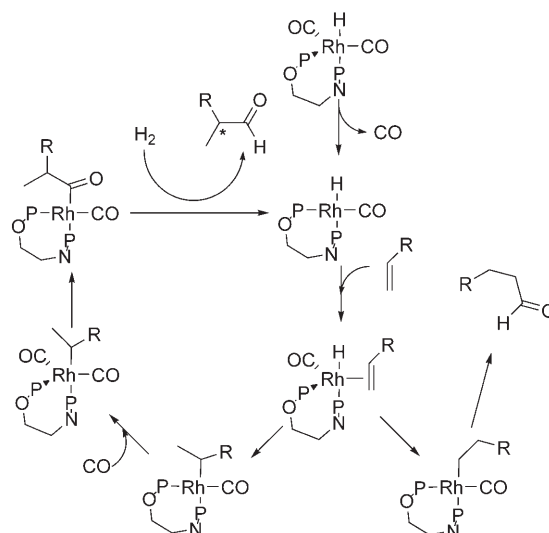
Mechanistic analysis: One of the main problems in theoretical studies on homogeneous catalysis is the growing number of coordination modes, conformations, and species to be

considered. Thus, some considerations need to be made to tackle the problem. Before presenting the results for styrene hydroformylation, we first discuss the possible selectivity-determining step, ligand coordination mode, and conformations of AMPP-type ligands.

First, in rhodium-catalyzed hydroformylation it is still unclear which are the rate- and selectivity-determining steps and whether they coincide.^[34–35] The fundamental catalytic steps of the generally accepted mechanism^[36] are represented in Scheme 3 for an AMPP ligand with equatorial/axial



Scheme 2.

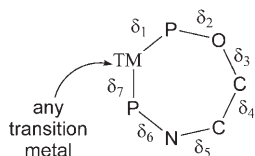


Scheme 3.

coordination. According to this mechanism, the selectivity for linear/branched and *R/S* branched products is determined in the alkene insertion, provided this step is irreversible. Previously, some of us showed that the relative energies of transition states for alkene insertion can be used to determine the regioselectivity for xantphos-type catalysts.^[21] In that case, with regard to regioselectivity, the relative stability of the different alkene complexes was unimportant, since each can give rise to pro-linear and pro-branched transition state and product. Others have also successfully used this kind of assumption in theoretical studies on the regioselectivity of hydroformylation.^[17–18, 22, 26–27] In the case of enantioselectivity, coordination of the alkene could also be the stereoselective step whenever alkene complexation is not reversible. The terminal alkene has two enantiofaces. Thus, each intermediate can only lead to one kind of pro-branched transition state, that is, pro-*R* or pro-*S*, depending on which face of the double bond coordinates to the metal. On the other hand, the interconversion of the different isomers of the styrene complex could be much faster than styrene insertion, and this would result in Curtin–Hammett behavior. Under this condition the product ratio would be therefore determined by the relative energy of the transition states for insertion.

Second, studies on hydrido complexes $[\text{HRh}(\text{AMPP})(\text{CO})_2]$ by in situ ^1H and ^{31}P NMR and IR spectroscopy under syngas pressure revealed that the coordination mode of the AMPP ligand could be related to the enantioselectivity.^[6] Ligands **a**, **b**, **e**, **h**, and **i** formed a single mononuclear hydrido complex which is in equilibrium with a catalytically inactive dinuclear carbonyl-bridged complex. In the mononuclear complexes, the ligand coordinates in equatorial/axial (**ea**) manner with the P(N) moiety in the axial position and the P(O) moiety in the equatorial position (see Scheme 2). On the other hand, ligands bearing electron-withdrawing groups in the phosphinite part give a mixture of several different species in solution. Interestingly, in complexes exhibiting fluxional behavior (**c** and **g**) the enantiomeric excess drops considerably as compared to complexes with equatorial/axial coordination (Table 1). In the case of pentacoordinate alkene complexes, we have computationally validated the preference for ligand coordination in $[(\text{AMPP})\text{RhH}(\text{CO})(\text{C}_2\text{H}_4)]$ (AMPP = ligand **a**, conformation **A**, see below). In principle, three different types of coordination isomers can be formed for equatorial coordination of ethene: equatorial/axial with the P(N) moiety in axial position (**ea1**), equatorial/axial with the P(N) moiety in equatorial position (**ea2**), and equatorial/equatorial (**ee**). For each type, two isomers can be defined according to position of ethene coordination in the **ea** forms, and the relative disposition of hydride and carbonyl ligands in the **ee** form. The most stable isomer was computed to be one of the **ea1** types, in full agreement with experimental findings for the corresponding dicarbonyl complexes. The calculated energies of the **ea2** and **ee** isomers are between 6 and 17 kJ mol⁻¹ higher than that of the lowest **ea1** isomer. These results suggest that the pentacoordinate species **ea** with the P(N) moiety in axial position might be responsible for good enantioselection, and therefore they are considered here. Furthermore, previous ab initio calculations have shown an axial preference of the hydride in related pentacoordinate TBP complexes, in which the alkene occupies an equatorial position and is oriented parallel to the equatorial plane.^[11–13]

Third, coordination of the AMPP ligand to the metal center forms a flexible seven-membered chelate ring, for which several conformations are conceivable. A search of the Cambridge Structural Database (CSD)^[37] was performed for metal complexes with the motif shown in Scheme 4 to determine the possible conformations of the AMPP chelate. The search produced 18 hits containing 26 molecular fragments. For each CSD hit seven endocyclic torsion angles δ_i ($i=1-7$) in the chelate ring (Scheme 4) were tabulated. Principal component analysis (PCA) was used to study the structural patterns in this dataset. The utility of PCA in identifying conformers of chelate complexes has been recently demonstrated.^[38] The PCA of the seven torsion angles gave two



Scheme 4.

principal components with large eigenvalues, which explained nearly 90% of the variance in the dataset. The scatter plot of the scores is shown in Figure 1. In this plot, it is

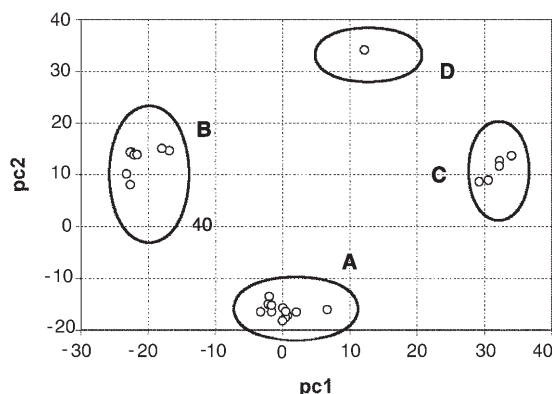


Figure 1. Scatter plot of pc1 and pc2 scores for the fragment described in Scheme 4.

possible to identify four different regions separated by unpopulated gaps. Each region, in which each point represents a particular AMPP fragment, corresponds to a distinct conformer of the ring (**A**, **B**, **C**, and **D**). The four types of ring conformation are schematically represented in Figure 2. In this case, PCA provides a significant reduction in dimensionality, and therefore it reduces the number of parameters needed to define the conformations of the AMPP fragment.

We evaluated the relative stabilities of the four conformations of the corresponding pentacoordinate ethene complexes $[(\text{AMPP})\text{RhH}(\text{CO})(\text{C}_2\text{H}_4)]$ in which AMPP is ligand **a** ($\text{R}=\text{CH}_3$). Note that for **ea** coordination of the AMPP ligand with the P(N) moiety in axial position *trans* to the hydride ligand, there are still two possible coordination posi-

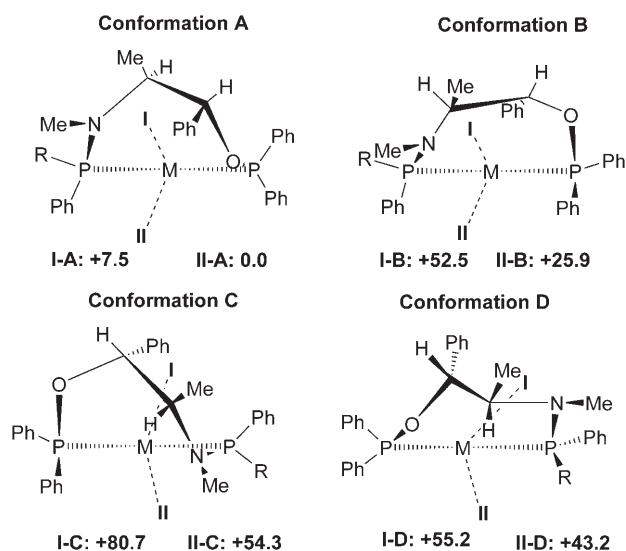


Figure 2. Schematic representation of conformation types (**A**, **B**, **C**, and **D**) found in X-ray structures for aminophosphane phosphinite seven-membered chelate rings.

tions for the alkene, **I** and **II** (Figure 2). At our computational level, the two most stable complexes are structures **I** and **II** of conformer **A**. The other isomers (**B**, **C**, and **D**) are notably higher in energy than their corresponding isomers **A** (between 26 and 73 kJ mol⁻¹). The highest energy isomers correspond to type **C** (Figure 2). All these structurally characterized fragments have an sp²-hybridized carbon atom in the seven-membered chelate ring, whereas the computed AMPP ligands only have sp³-hybridized carbon atoms. On the other hand, the group of lowest energy **A**-type conformations includes the structure that most resembles the ligand under analysis. The entry IHEKUB corresponds to a ruthenium complex with an EPHOS ligand ((+)-(1*R*,2*S*)-2-[(diphenylphosphanyl)methylamino]-1-phenylpropyl diphenylphosphinite) analogous to ligand **h**.^[59] From all these data, we presume that the species involved in enantioselection (styrene complexes and transition states for styrene insertion) with ring conformations **B**, **C**, and **D** are shifted upward in energy with respect to the **A** conformations, and therefore their contribution to overall enantioselectivity can be neglected.

In summary, for **ea** coordination of the AMPP ligand there are two available equatorial coordination positions for the alkene, **I** and **II**. Thus, the alkene substituent can adopt four different orientations. From each conformation the alkene can rotate clockwise (CW) or counterclockwise (CCW), that is, rotation through the phosphinite or carbonyl sides (labeled with **P** and **CO** superscripts, respectively) to reach the pro-linear and pro-branched TSs (see Figure 3). Since we are only interested in analyzing the enantioselectivity, we will not consider the pro-linear TSs. Thus, the number of possible pathways is eight, four of which lead to the *R* product

(**R**), and four to the *S* product (**S**). Consequently, eight styrene complexes and eight TSs must be computed. Figure 3 depicts schematically the pathways and their labels. The structures discussed hereafter are labeled, for example, as **2a-II-S^P**, with the following meaning: 1) The first label such as **2a** indicates the type of species [ethene complex (**1**), styrene complex (**2**), or transition state for styrene insertion (**TS**)] and type of ligand (**a**, **h**, **i**, or **j**). 2) The second label, **I** or **II**, indicates the two different equatorial positions for alkene coordination. 3) The third label, **S^P**, **S^{CO}**, **R^P**, or **R^{CO}**, indicates which enantioface of the double bond is bound to the metal and the orientation of the phenyl substituent.

P-chiral versus P-nonchiral ligands: Initially, we focus on AMPP ligands **a** (R=CH₃) and **h** (R=Ph), which respectively represent the case of a ligand with a stereogenic center at the phosphorus atom and the case without a stereogenic center. For ligand **a**, we characterized the eight possible paths by localization of the corresponding styrene complexes and transition states. Table 2 collects the relative energies and the main geometric parameters of all the characterized structures. The energies are relative to that of the lowest lying styrene complex and transition state. The decomposition of total energy in quantum mechanics (*E*_{QM})

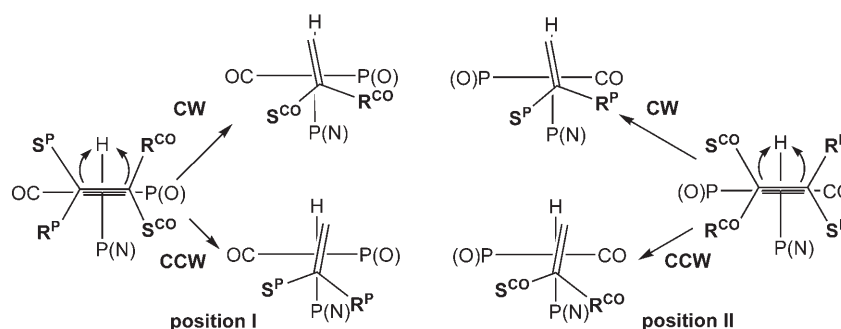


Figure 3. Definition of the possible paths leading to branched product from the key equatorial/axial pentacoordinate intermediate.

Table 2. Relative energies [kJ mol⁻¹] and selected geometric parameters (distances [Å] and angles [°]) of the styrene complexes and transition state for styrene insertion for ligands **a** (P-stereogenic) and **h** (P-nonstereogenic)^[a].

Styrene	Ligand a								Ligand h			
	S ^{CO}	R ^{CO}	S ^P	R ^P	S ^{CO}	R ^{CO}	S ^P	R ^P	Position II S ^{CO}	R ^{CO}	S ^P	R ^P
<i>E</i> _{total}	16.8	3.9	20.6	20.5	0.0	3.6	5.1	9.8	0.0	5.3	9.5	12.8
<i>E</i> _{QM}	10.4	8.2	1.1	6.9	0.0	7.0	-1.7	-3.1	0.0	13.0	4.4	3.3
<i>E</i> _{MM}	6.4	-4.3	19.6	13.7	0.0	-3.4	6.8	12.9	0.0	-7.7	5.1	9.5
Rh-H	1.590	1.587	1.591	1.586	1.593	1.592	1.596	1.597	1.586	1.590	1.590	1.595
C _α =C _β	1.418	1.414	1.417	1.415	1.416	1.419	1.415	1.418	1.420	1.419	1.416	1.413
TS	S ^{CO}	R ^{CO}	S ^P	R ^P	S ^{CO}	R ^{CO}	S ^P	R ^P	S ^{CO}	R ^{CO}	S ^P	R ^P
<i>E</i> _{total}	13.1	18.7	9.3	14.9	0.0	13.7	2.3	12.7	5.4	5.6	3.1	0.0
<i>E</i> _{QM}	-1.2	-2.8	0.5	8.8	0.0	1.4	1.6	-1.7	6.4	5.0	5.8	0.0
<i>E</i> _{MM}	14.3	21.4	8.8	6.2	0.0	12.3	0.7	14.4	-1.0	0.6	-2.7	0.0
H-Rh-C _α -C _β	22.0	23.0	-12.1	-8.2	-9.6	-9.7	4.1	12.6	-8.9	-10.7	4.0	13.6
Rh-H	1.640	1.641	1.649	1.648	1.643	1.639	1.654	1.648	1.635	1.644	1.652	1.646
C _α =C _β	1.427	1.427	1.418	1.422	1.407	1.407	1.422	1.415	1.408	1.411	1.418	1.416

[a] C_α=styrene terminal carbon atom; C_β=styrene substituted carbon atom.

and molecular mechanics (E_{MM}) parts is also reported in Table 2.

Two main features are clear from the results of calculations on ligand **a**. First, the lowest energy minimum and saddle point correspond to position **II**, the **2a-II-S^{CO}** styrene complex and the **TSa-II-S^{CO}** transition state. Although some low-energy species correspond to position **I**, it seems that the preferred position for styrene coordination and insertion is position **II**, since on a one-to-one basis the isomers of position **II** are lower in energy than their position **I** counterparts. Second, in both styrene coordination and styrene insertion through path **II**, the pro-*S* species are energetically favored over the pro-*R* ones, by 0.0 and 5.1 versus 3.6 and 9.8 kJ mol⁻¹ for styrene complexes, and 0.0 and 2.3 versus 13.7 and 12.7 kJ mol⁻¹ for transition states. This initial energetic analysis agrees with the configuration of the experimentally observed product. However, at this point, it is not possible to establish whether the enantioselectivity-determining step is styrene coordination or styrene insertion.

The overall *S* selectivity of the reaction is intimately related to the fact that it passes through position **II**. Thus, if the reaction proceeded through paths **I** and styrene coordination were the enantioselectivity-determining step, the main product would be the *R* isomer, whereas if the determining step were styrene insertion, there would be a significant reduction in stereodifferentiation. Note that the energy differences between the corresponding pro-*S* and pro-*R* TSs in path **I** of around 5 kJ mol⁻¹ are significantly smaller than those on path **II** (≥ 10 kJ mol⁻¹). Thus, a priori, we focus our discussion on the nature of this position and the factors defining its preference. It does not matter at this point whether there are other possible conformations and/or coordination modes defining new reaction paths, whenever these are not more favored than those through position **II**.

To compare ligand **a** with the case of a ligand without a stereogenic center at the phosphorus atom, we investigated path **II** for ligand **h** (R=Ph). The relative energies of the pro-*S* and pro-*R* styrene complexes with ligands **a** and **h** show similar patterns (Table 2), despite the fact that experimentally **a** exhibited significant stereinduction and **h** did not. On the other hand, computation of relative energies of TSs for alkene insertion reproduce experimental enantioselectivity trends. The pro-*S* TSs are energetically favored with respect to the pro-*R* ones for ligand **a** (P-stereogenic). The relative energies of the pro-*R* transition states lie 13.7 and 10.4 kJ mol⁻¹ above their pro-*S* counterparts for ligand **a**. On going from ligand **a** to **h** (P-nonestereogenic) there is a substantial reduction of energy differences. In **h** the maximum difference between a pro-*S* and a pro-*R* TS is only 3.1 kJ mol⁻¹. Thus, the results for styrene insertion fully agree with experimental observations indicating that styrene insertion through path **II** determines the enantioselectivity rather than styrene coordination.

The structural nature of the transition states for position **II** is also fully consistent with experimental findings, for which high *ee* values were obtained for the system with an asymmetric center at the phosphorus atom. A closer look at

the geometries of the TSs for ligands **a** and **h** reveals that the phenyl substituent of the olefinic substrate faces the substituents of the P-stereogenic atom. In **a**, the styrene substituent faces the phenyl group of the aminophosphane phosphorus atom for the pro-*S* TSs, while it faces the methyl substituent on the phosphorus atom for the pro-*R* isomers (Figure 4). It seems that the different interaction of

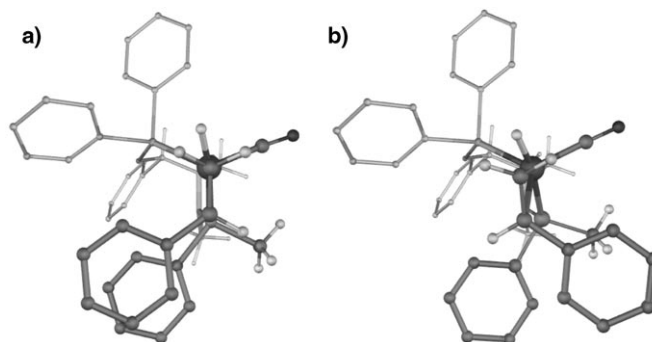


Figure 4. Molecular structures of pro-*S* and pro-*R* TSs for styrene insertion with ligand **a**: **TSa-II-S^{CO}** (a) and **TSa-II-R^{CO}** (b). Hydrogen atoms of phenyl groups are omitted for clarity.

styrene with the P(N)* substituents is responsible for stereodifferentiation. Accordingly, for path **TSa-II** the energy differences between pro-*S* and pro-*R* TSs lie mostly in the MM part. Note that in the QM/MM partition scheme, the substituents of the olefinic substrate and of the phosphorus atom are included in the MM part. In **h**, the methyl group is replaced by a phenyl group. Thus, in the pro-*S* and pro-*R* TSs the substrate points toward the same type of ligand substituent, and consequently similar type of interactions are expected for both TSs.

Despite the widely accepted idea that the stereoiduction in asymmetric hydroformylation is determined in alkene coordination, these results indicate that styrene insertion into the rhodium–hydride bond is the selectivity-determining step. In this case, there is a loss of stereochemical memory through rapid conformational interconversion of styrene complexes. Thus, Curtin–Hammett behavior is operative, and therefore it is the relative energies of transition states for alkene insertion that determine selectivity. In line with these arguments, recent high-level calculations on related model systems showed that barriers for alkene association/dissociation are negligible, and when free-energy corrections are considered, alkene complexes and their dissociation products are almost isoenergetic.^[14]

Substrate–ligand interactions: To more deeply analyze the factors governing enantioselectivity, we investigated ligand–substrate interactions in more detail. We stated above that the difference between phenyl–phenyl and phenyl–methyl interactions may be crucial in stereodifferentiation. Structural inspection allowed us to identify two aryl rings in face-to-face arrangement for pro-*S* TSs of path **II** with ligand **a**, and

an alkyl C–H bond oriented towards an aryl ring for pro-*R* TSs of path **II** with ligand **a**. Noncovalent interactions involving aromatic rings such as π – π stacking and C–H/ π interactions are well characterized, both experimentally^[40–41] and theoretically.^[42–46] Their importance has been demonstrated for many chemical and biological processes, including molecular recognition. Their occurrence in asymmetric catalysis has been successfully characterized and evaluated by QM/MM methods.^[47–48] However, the role of arene–arene and arene–alkyl interactions is still a matter of debate.

Quantifying the contribution of individual functional groups to catalysis is not an easy task. However, theoretical methods allow the design of artificial models to estimate the importance of each individual molecular fragment. To evaluate the relative strengths of phenyl–phenyl π – π stacking and alkyl–phenyl C–H/ π interactions, we built two model systems by assembling the following

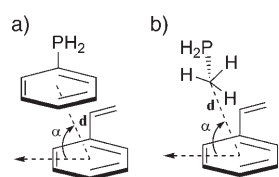


Figure 5. Schematic representation of model interacting fragments styrene–PH₂Ph (a) and styrene–PH₂CH₃ (b) for π – π stacking and C–H/ π interactions in ligand **a**. Distance d between ring centroids (a), and between ring centroid and carbon atom (b). Angle α between ring mean planes (a) and between ring mean plane and centroid–carbon vector (b).

interacting moieties (Figure 5): 1) styrene and PH₂Ph, and 2) styrene and PH₂(CH₃). Each moiety was treated at the same level as for the whole complex, that is, with inclusion of the phenyl and methyl substituents in the MM part. The interaction energies (IE) were evaluated as the energy difference between the two fragments in the transition-state geometries and the two fragments at infinite distance in the geometries they adopt at the saddle points. Table 3 collects the energies and geometric parameters (Figure 5) of these interactions for path **II** of

ligand **a**. The interaction energies for pro-*S* TSs are stabilizing in nature, whereas for pro-*R* TSs the IEs are negligible or even slightly repulsive. High-level theoretical studies on benzene dimer proposed the existence of different minima: T-shaped, parallel, and parallel-displaced.^[43–44] The last two minima have ring–center distances of around 3.8 and 3.9 Å, respectively. Calculations at a similar level for benzene–methane models obtained intermolecular distances between

methane carbon atom and benzene centroid of 3.6–4.0 Å, depending on methane orientation.^[42] The distances between the ring centroids for the pro-*S* TSs (3.1 Å) are significantly shorter than those of previous studies on benzene dimer. However, at our molecular mechanics level, the distance in global minimum for π – π interaction of the benzene dimer (3.111 Å) is very similar to those at TSs. Moreover, optimization of the styrene–PH₂Ph adduct leads to a close stable structure with an inter-ring distance of 3.193 Å, and to a similar interaction energy of –21.1 kJ mol^{–1}. These data suggest that the substrate is arranged in a way that maximizes its π – π stacking interaction with the catalyst. In the case of pro-*R* TSs, the distances between the methyl carbon atom and the phenyl centroid range from 3.6 to 4.0 Å in **TSa-II-R^{CO}** and **TSa-II-R^P**, respectively. The distance is 3.644 Å for the optimized styrene–methylphosphane adduct and 3.244 Å for the benzene–methane model complex, the interaction energies of which are –7.5 and –8.9 kJ mol^{–1}, respectively. In accordance with previous studies,^[42] the structural analysis might indicate a very shallow potential energy curve and a weak interaction for phenyl–methyl groups, and consequently the substrate–ligand interactions in pro-*R* TSs do not seem to play a relevant role.

A clear correlation exists between the computed IEs of the functional groups and the relative energies of the TSs (Table 3). More interestingly, the computed IEs account for most of the energy differences observed between the pro-*S* and pro-*R* TSs. The IEs for pro-*S* TSs are about 15 kJ mol^{–1}, whereas for pro-*R* TSs the IEs are practically negligible. The difference between the IEs for pro-*S* and pro-*R* TSs (about 15 kJ mol^{–1}) are roughly their difference in relative energies (about 12 kJ mol^{–1}). Thus, we can conclude that stereodifferentiation is governed by weak-type interaction induced in the different interactions of styrene with the substituents at the stereogenic P(N)* center (phenyl and methyl). Furthermore, no significant effect on enantioselectivity of the other two chiral centers at the AMPP backbone seems to be present.

Assuming a Boltzmann distribution, the *ee* obtained from the relative energies of TSs of position **II** is calculated to be 98.6% for the *S* isomer. Our computed *ee* value overestimates the experimentally determined enantioselectivity of 75% under optimal conditions. The computed MM interaction energies of benzene dimer and benzene–methane adduct are –22.6 and –8.9 kJ mol^{–1}, respectively. The MM calculations tend to overestimate the IE values found at higher computational level (from –10.4^[43] to –11.7^[44] and –6.7 kJ mol^{–1}^[42], respectively) and experimental measurements in the gas phase on benzene dimer (from –6.7 ± 0.8 kJ mol^{–1}^[49] to –10.0 ± 1.6 kJ mol^{–1}^[50]). However, the differences between π – π stacking and C–H/ π interactions is qualitatively reproduced by MM calculations, which favor the interaction between two phenyl groups. Thus, MM treatment of π – π stacking interactions could be one of the main reasons for the overestimation of *ee* in our calculation. Note that in transition-state calculations the substituents on the alkene and on the phosphorus atom are included in the MM

Table 3. Relative energies E_{rel} [kcal mol^{–1}] of transition states for path **II**, ligand **a**. Interaction energies (IE [kcal mol^{–1}]) between substrate and the key ligand moieties in the model systems. Distance between ring centroids and between ring centroid and carbon atom (d in Å). Angle between ring mean planes and between ring mean plane and centroid–carbon vector (α [°], see Figure 5).

	styrene-PH ₂ Ph		styrene-PH ₂ CH ₃	
	TSa-II-S^{CO}	TSa-II-S^P	TSa-II-R^{CO}	TSa-II-R^P
E_{rel}	0.0	2.3	13.7	12.7
IE	–15.1	–15.9	–1.4	2.2
d	3.139	3.068	3.634	4.007
α	72.0	80.1	77.0	64.3

region, and their interactions govern stereodifferentiation. In fact, if we apply a correction factor, derived from comparison with higher level calculations,^[51] to the relative energies of pro-*S* TSs, the calculated *ee* drops to about 74%, which is close to the experimental results. The value resulting from the application of the correction factor is an approximation, and it must be interpreted qualitatively. However, it clearly shows a meaningful trend in which the theoretical *ee* is in better agreement with experimental findings.

We recomputed the **TSa-II-S^{CO}** and **TSa-II-R^{CO}** structures at full DFT level. On going from QM/MM to full DFT calculation the energy difference between the two isomers decreases substantially, and the pro-*R* TS is more stable than the pro-*S* TS by 2.6 kJ mol⁻¹. Computation of interaction energies of the styrene–phenylphosphane and the styrene–methylphosphane fragments by an analogous procedure to that described above yielded values of 1.3 and –1.9 kJ mol⁻¹, respectively, which are fully consistent with the relative stabilities of the TSs. Thus, according to full DFT calculations, no significant stereoinduction is expected for interaction of the substrate with the stereogenic center at the phosphorus atom. This is in agreement with previous theoretical findings, which suggest that dispersion forces cannot be properly described by gradient-corrected density functional approaches because this interaction is a long-range nonlocal correlation effect.^[46,52] In fact, systematic DFT studies on intermolecular binding of benzene dimer predict weak attractive or repulsive interactions.^[45–46] As in previous findings, the interaction energies of benzene dimer and benzene–methane adduct computed at our density functional level are –5.5 and –4.1 kJ mol⁻¹, respectively. These values, compared to those of CCSD(T) calculations (–10.4 and –6.1 kJ mol⁻¹, respectively),^[42–43] show that DFT underestimates IEs and, more importantly, that the difference between π – π stacking and C–H/ π interactions is minimized by DFT. On the other hand, molecular mechanics methods can easily describe long-range dispersion-type interactions via a classical potential such as Lennard–Jones 12-6 potential. Thus, in this case, in which the π – π stacking interactions are crucial for stereodifferentiation, the DFT/MM calculations tend to give superior results to pure DFT calculations.

Stereochemical model: We have succeeded in reproducing experimental trends and in identifying and evaluating the key factors which govern the enantioselectivity. To help to rationalize the stereochemical outcome of AMPP ligand systems, we built a stereochemical model from simple schematic representations. Using this scheme, we rediscuss the results in order to provide a more general understanding of the mechanism. In a first approximation, we assume that the reaction proceeds mostly through path **II**. The rationalization of the observed *ee* values with ligands **a** and **h** are based on the model depicted in Figure 6. The (O)P–Rh–CO and (N)P–Rh–H axes of the system are projected into the plane of the paper, and the alkene is at the front side. The arrows indicate the main intramolecular interactions between substrate and catalyst.

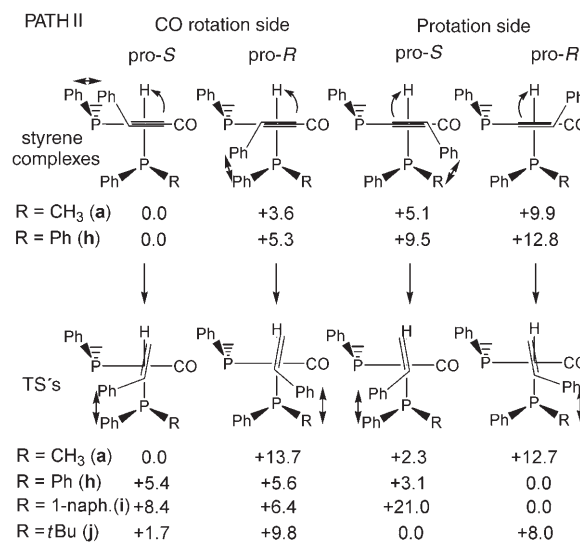


Figure 6. Relative energies and schematic representation of styrene complexes and transition states for styrene insertion in path **II**. Energies [kJ mol⁻¹] relative to the lowest energy styrene complex or transition state. Double arrows indicate the main intramolecular ligand–substrate interactions, and single arrows indicate the direction of rotation of styrene to reach the transition state.

For styrene complexes, both pro-*S* and pro-*R* species of the carbonyl-rotation side exhibit stabilizing phenyl–phenyl interactions. Accordingly, the calculated energies are similar for both species in ligand **a** and **h**. In the pro-*S* species of the phosphinite-rotation side, the substrate interacts mostly with the R substituent of the P(N) atom. This might favor *S* configuration in ligand **h** by means of a stabilizing phenyl–phenyl interaction. However, the computed relative energies indicate that the interaction is less effective for this isomer. Finally, no significant stabilizing interaction is observed in the pro-*R* isomers of the phosphinite-rotation side, and consequently they are the highest in energy. From this model, we would expect a very low enantioselectivity for both **a** and **h** ligands, and an even higher preference for the *S* isomer with ligand **h**. This is contrary to experimental observations, and consequently it seems that coordination of styrene can be rejected as the enantioselectivity-determining step. In the TSs for styrene insertion yielding the branched product, two types of substrate–ligand interactions are possible. For pro-*S* TSs the styrene substituent interacts with the phenyl substituent of P(N), whereas for pro-*R* TSs styrene interacts with the R substituent of P(N). Thus, when R is a methyl group (ligand **a**) the difference in interaction induces enantioselectivity. When R is a phenyl group (ligand **h**) the substrate–ligand interactions for both types of transition state become very similar, and consequently we do not expect high stereoinduction. According to the proposed stereochemical model, the enantioselectivity of this reaction could, in principle, be tuned by appropriate selection of the substituents on the aminophosphane phosphorus atom.

To validate our mechanism, we tested it on the enantioselectivity of ligand **i** (R = 1-naphthyl). Experimental data in-

indicated that the introduction of a 1-naphthyl group resulted in a considerable decrease in enantioselectivity to only 10%, despite the presence of a stereogenic center at the phosphorus atom. A possible explanation is that phenyl–phenyl and phenyl–naphthyl interactions are of the same order of magnitude. However, the calculated interaction energy between styrene and the $\text{PH}_2(1\text{-naphthyl})$ model fragment ($-38.5 \text{ kJ mol}^{-1}$) is significantly higher than that for the styrene– PH_2Ph adduct ($-21.1 \text{ kJ mol}^{-1}$). Moreover, the pro-*R* TSs are energetically favored with respect to the pro-*S* TSs (see Figure 6), which would indicate reversal of enantioselectivity favoring the *R* product. These data suggest that the proposed stereochemical model is mistaken or incomplete. Therefore, we computed the transition states for path **I**, and this showed that the pro-*S* TSs are slightly more stable than the corresponding pro-*R* TSs of path **II**. Setting the zero of energy to the most stable isomer of path **II**, the relative energies of pro-*S* TSs are -2.7 and -0.8 kJ mol^{-1} for **TSi-I-S^{CO}** and **TSi-I-S^P**, respectively, whereas the pro-*R* TSs showed relative energies of 12.9 and 17.8 kJ mol^{-1} for **TSi-I-R^{CO}** and **TSi-I-R^P**, respectively. These values indicate that the two pro-*S* TSs of path **I** contribute significantly to the overall enantioselectivity, balancing the *R* preference predicted by path **II**. Thus, calculations predict a small overall *S* preference, in agreement with experimental results. A simple schematic representation for path **I** (Figure 7, analo-

path **I**. As a general rule, we can state that asymmetric substitution of the P(N) atom induces enantioselectivity whenever the functional groups at the *R* position do not exhibit a higher (or similar) stabilizing interaction with the substrate than the other phosphorus substituent.

Novel ligand systems: The utility of computationally derived stereochemical models lies not only in the analysis of well-known aminophosphane phosphinites, but also in the search for novel ligand systems. The synthetic route to the aminophosphane phosphinite ligand family provides enormous potential for variation, including diastereoselective introduction of various residues on the phosphorus moieties.^[6,9] Our initial target phosphane for further computational study is a simple derivative of ligand **a** in which the methyl substituent at the stereogenic phosphorus atom has been replaced by the bulkier *t*Bu group. According to the proposed stereochemical model, we expected that the hypothetical ligand **j** ($R = t\text{Bu}$) would destabilize the pro-*R* TSs of path **II**, and consequently cause a higher preference for pro-*S* species. For ligand **j**, the computed TSs of path **II** show a preference for pro-*S* TSs, but we do not observe a qualitative difference with respect to the experimentally tested ligand **a** (Figure 6). Thus, despite introducing a more bulky substituent, which should in principle destabilize the corresponding pro-*R* TSs, the AMPP skeleton is flexible enough to accommodate styrene. In other words, the ligand can rearrange to optimize the distance between a C–H moiety of the *t*Bu group and the phenyl ring of styrene. On going from ligand **a** to **h**, we observed variation of the dihedral angles involving the Rh–P(N) and P–N bonds of about 10° in the TSs. In fact, the calculated interacting energies of the model functional groups styrene and $\text{PH}_2(t\text{Bu})$ are slightly attractive: -3.8 and -2.3 kJ mol^{-1} for **TSj-II-R^{CO}** and **TSj-II-R^P**, respectively.

Recently, Yoon and Jacobsen introduced the concept of privileged ligands for asymmetric catalysis.^[53] These are ligand structures which have broad applicability across many different types of reaction. These authors suggest that common feature of such ligands could be that they usually have rigid structures. Here, our analysis of the AMPP ligand family reveals that its flexible backbone allows the stereorecognition of one enantiomer, but prevents severe stereohindrance of the other enantiomer. Thus, a possible strategy to develop more efficient catalysts for asymmetric hydroformylation and other enantioselective processes could be to design related ligands with more rigid backbones. This would allow stereorecognition and stereohindrance to be combined and stereodifferentiation to be increased. Within the AMPP family, another possible strategy could be to replace the phenyl substituent at the stereogenic phosphorus atom by a functional group which would reinforce the stabilizing interaction with the substrate observed in the pro-*S* TSs. For example, we have already observed that the 1-naphthyl group exhibits a stronger π – π stacking interaction with styrene than the phenyl residue of ligand **a**.

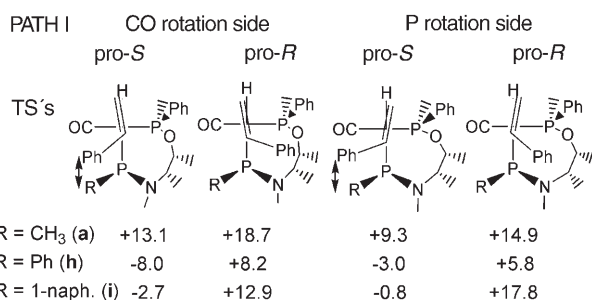


Figure 7. Relative energies and schematic representation of transition states for styrene insertion on path **I**. Energies [kJ mol^{-1}] relative to the lowest energy transition state. Double arrows indicate the main intramolecular ligand–substrate interactions.

gous to that of path **II**) reveals a stabilizing phenyl–naphthyl interaction for pro-*S* TSs, whereas the pro-*R* TSs do not exhibit any significant interaction. In agreement with this, for ligand **h** we observe a similar pattern due to a stabilizing phenyl–phenyl interaction, whereas for ligand **a** all TSs are shifted upward in energy with respect to the lowest isomer of path **I**, due to the absence of significant stabilizing interactions (see Figure 7).

In summary, the interaction of the substrate with substituents at the P-stereogenic center governs the enantioselectivity. However, the rationalization of the stereochemical outcome is not that straightforward because the interaction of the substrate with the *R* substituent favors/disfavors both the *R* product through path **II** and the *S* product through

Summary and Conclusions

Our calculations reproduce experimental results showing that alkene insertion into the rhodium–hydride bond is the step determining the enantioselectivity, and not alkene coordination. Analysis of ligand–substrate interactions in the transition states for styrene insertion indicates that different weak nonbonding interactions of styrene with the substituents at the stereogenic P(N)* center are responsible for stereodifferentiation. In the case of ligand **a**, the difference between phenyl–phenyl π – π -stacking interaction and methyl–phenyl C–H/ π interactions governs enantioinduction. The stronger π – π stacking interaction stabilizes the pro-*S* transition states and favors the *S* product. Thus, on going from ligand **a** (P-stereogenic) to **h** (P-nonstereogenic) the ligand–substrate interactions at pro-*S* and pro-*R* TSs become very similar, and consequently low *ee* is expected. In fact, the situation is a little more complicated because it is necessary to consider two coordination modes **I** and **II** (Figures 6 and 7, respectively). When the interaction of the R substituent of the aminophosphane phosphorus atom with the substrate is stabilizing in nature, the reaction path through coordination mode **I** becomes available. Then, paths **I** and **II** exhibit opposite asymmetric inductions that cause cancellation of stereoselectivity, as is the case for ligand **i** (R=1-naphthyl). On the other hand, the chirality of the AMPP backbone plays a secondary role in asymmetric hydroformylation, possibly favoring a specific ligand conformation.

We have built a stereochemical model based on simple molecular schematic representations (Figures 6 and 7) in order to rationalize the observed stereochemical outcome and to search for novel ligand systems. According to the proposed stereochemical model, to improve the performance we should avoid functional groups at the R position that undergo stabilizing interaction with the substrate. Thus, a novel ligand **j** with a potentially destabilizing *t*Bu substituent at R position was envisaged and computationally tested. However, no relevant selective stereohindrance was observed because of the flexible AMPP backbone. From these results, two strategies can be envisaged for the development of more efficient AMPP or derived catalysts. First, efforts could be directed towards the design of related ligands with more rigid backbones, to combine stereorecognition and stereohindrance at the asymmetric phosphorus atom. Second, the replacement of the phenyl substituent at the P(N)* atom by a functional group that reinforces the interaction with the substrate would improve stereodifferentiation. By comparing the molecular structure of enantioselective Rh/AMPP and Rh/BINAPHOS catalysts, we can preliminarily outline some prerequisites for efficient enantioinduction in asymmetric hydroformylation of styrene: 1) ligands with a well-defined coordination mode and 2) ligands with functional groups providing strong ligand–substrate stereorecognition. Currently, our experimental laboratory is working on the synthesis of novel ligands for asymmetric catalysis based on the insight gained in this theoretical

study. Also, theoretical analysis of other asymmetric ligands is underway.

Finally, quantum mechanics/molecular mechanics methods have shown their potential applicability to the study of homogeneous catalyst systems. In this case, where nonbonding π – π stacking interactions govern enantioselectivity, QM/MM gives better results than pure DFT quantum mechanics methods.

Acknowledgement

The authors are grateful to the Ministerio de Educación y Tecnología for financial support with the reference BQU2002-04110-C02-01, and from the CIRIT of the Generalitat de Catalunya under the project SGR01-00315. We thank the ICIQ Foundation for financial support. We also thank Dr. Christian Müller for his valuable comments on the revision of the manuscript.

- [1] a) I. Ojima, *Catalytic Asymmetric Synthesis*, Wiley-VCH, New York, **2000**; b) E. N. Jacobsen, A. Pfaltz, H. Yamamoto, *Comprehensive Asymmetric Catalysis*, Springer, New York, **1999**; c) G. C. Fu in *Transition Metals for Organic Synthesis: Building Blocks and Fine Chemicals*, Vol. 2, (Eds.: M. Beller, C. Bolm), Wiley-VCH, Weinheim, **1998**.
- [2] a) F. Agbossou, J. -F. Carpentier, A. Mortreux, *Chem. Rev.* **1995**, *95*, 2485–2506; b) C. Claver, P. W. N. M. van Leeuwen, *Asymmetric Hydroformylation in Rhodium Catalyzed Hydroformylation* (Eds.: P. W. N. M. van Leeuwen, C. Claver), Kluwer-CMC, Dordrecht, **2000**, pp. 107–144; c) B. Breit, W. Seiche, *Synthesis* **2001**, 1–36; d) B. Breit, *Acc. Chem. Res.* **2003**, *36*, 264–275.
- [3] N. Sakai, S. Mano, K. Nozaki, H. Takaya, *J. Am. Chem. Soc.* **1993**, *115*, 7033–7034.
- [4] a) J. E. Babin, G. T. Whiteker, WO 93/03830, **1992**. b) G. J. H. Buisman, L. A. van der Veen, A. Klootwijk, W. G. J. der Lange, P. C. J. Kamer, P. W. N. M. van Leeuwen, D. Vogt, *Organometallics* **1997**, *16*, 2929–2939; c) M. Diéguez, O. Pàmies, A. Ruiz, S. Castillón, C. Claver, *Chem. Eur. J.* **2001**, *7*, 3086–3094; d) C. J. Cobley, K. Gardner, J. Klosin, C. Praquin, C. Hill, G. T. Whiteker, A. Zanotti-Gerosa, J. L. Petersen, K. A. Abboud, *J. Org. Chem.* **2004**, *69*, 4031–4040; e) C. J. Cobley, J. Klosin, C. Qin, G. T. Whiteker, *Org. Lett.* **2004**, *6*, 3277–3280.
- [5] G. Franciò, G. Faraone, W. Leitner, *Angew. Chem.* **2000**, *112*, 1486–1488; *Angew. Chem. Int. Ed.* **2000**, *39*, 1428–1430; .
- [6] R. Ewalds, E. B. Eggeling, C. H. Alison, P. C. J. Kamer, P. W. N. M. van Leeuwen, D. Vogt, *Chem. Eur. J.* **2000**, *6*, 1496–1506.
- [7] For example: a) S. Breeden, D. J. Cole-Hamilton, D. F. Foster, G. J. Schwarz, M. Wills, *Angew. Chem.* **2000**, *112*, 4272–4274; *Angew. Chem. Int. Ed.* **2000**, *39*, 4106–4108; b) B. Breit, G. Heckmann, S. K. Zahn, *Chem. Eur. J.* **2003**, *9*, 425–434; c) T. P. Clark, C. R. Landis, S. L. Freed, J. Klosin, K. A. Abboud, *J. Am. Chem. Soc.* **2005**, *127*, 5040–5042.
- [8] a) M. Petit, A. Mortreux, F. Petit, G. Buono, G. Pfeiffer, *New J. Chem.* **1983**, *7*, 583–586; b) E. Cesarotti, A. Chiesa, G. D'Alfonso, *Tetrahedron Lett.* **1982**, *23*, 2995–2996; c) G. Pracejus, H. Pracejus, *J. Mol. Catal.* **1984**, *24*, 227–230.
- [9] For some reviews, see a) F. Agbossou, J. -F. Carpentier, F. Hapiot, I. Suisse, A. Mortreux, *Coord. Chem. Rev.* **1998**, *178–180*, 1615–1645; b) F. Agbossou-Niederborn, I. Suisse, *Coord. Chem. Rev.* **1998**, *242*, 145–158.
- [10] Some recent references a) I. Cesarotti, I. Rimoldi, *Tetrahedron: Asymmetry* **2004**, *15*, 3841–3845; b) N. V. Dubrovina, V. I. Tararov, Z. Kadyrova, A. Monsees, A. Boerner, *Synthesis* **2004**, *12*, 2047–2051.

- [11] J. J. Carbó, F. Maseras, C. Bo, *Rhodium Diphosphine Hydroformylation in Computational Modeling of Homogenous Catalysis* (Eds.: F. Maseras, A. Lledós), Kluwer Academic Publishers, Dordrecht, **2002**.
- [12] a) S. Niu, M. B. Hall, *Chem. Rev.* **2000**, *100*, 353–406; b) M. Torrent, M. Solà, G. Frenking, *Chem. Rev.* **2000**, *100*, 439–494; c) T. R. Cundari, *Computational Organometallic Chemistry*, Marcel Dekker, New York, **2001**.
- [13] a) N. Koga, K. Morokuma, *Chem. Rev.* **1991**, *91*, 823–842; b) D. G. Musaev, K. Morokuma, *Adv. Chem. Phys.* **1996**, *XCV*, 61–128.
- [14] D. Gleich, J. Hutter, *Chem. Eur. J.* **2004**, *10*, 2435–2444.
- [15] S. A. Decker, T. R. Cundari, *Organometallics* **2001**, *20*, 2827–2841.
- [16] T. Matsubara, N. Koga, Y. Ding, D. G. Musaev, K. Morokuma, *Organometallics* **1997**, *16*, 1065–1078.
- [17] a) W. R. Rocha, W. B. de Almeida, *Int. J. Quantum Chem.* **2000**, *78*, 42–51; b) W. R. Rocha, W. B. de Almeida, *J. Mol. Struct. (THEOCHEM)* **2003**, *634*, 95–106.
- [18] a) G. Alagona, C. Ghio, R. Lazzaroni, R. Settambolo, *Organometallics* **2001**, *20*, 5394–5404; b) G. Alagona, C. Ghio, R. Lazzaroni, R. Settambolo, *Inorg. Chim. Acta* **2004**, *357*, 2980–2988.
- [19] a) F. Maseras, K. Morokuma, *J. Comput. Chem.* **1995**, *16*, 1170–1179; b) F. Maseras, *Chem. Commun.* **2000**, 1821–1827.
- [20] a) M. Svensson, S. Humbel, R. D. J. Froese, T. Matsubara, S. Sieber, K. Morokuma, *J. Phys. Chem.* **1996**, *100*, 19357–19363; b) S. Dapprich, I. Komaromi, K. S. Byun, K. Morokuma, M. J. Fisch, *J. Mol. Struct. (THEOCHEM)* **1999**, *461–462*, 1–21.
- [21] J. J. Carbó, F. Maseras, C. Bo, P. W. N. M. van Leeuwen, *J. Am. Chem. Soc.* **2001**, *123*, 7630–7637.
- [22] S. A. Decker, T. R. Cundari, *J. Organomet. Chem.* **2001**, *635*, 132–141.
- [23] S. A. Decker, T. R. Cundari, *New J. Chem.* **2002**, *26*, 129–135.
- [24] C. R. Landis, J. Uddin, *J. Chem. Soc. Dalton Trans.* **2002**, 729–742.
- [25] a) L. A. Castonguay, A. K. Rappé, C. J. Casewit, *J. Am. Chem. Soc.* **1991**, *113*, 7177–7183; b) C. P. Casey, L. M. Petrovich, *J. Am. Chem. Soc.* **1995**, *117*, 6007–6014; c) R. Paciello, L. Siggel, M. Röper, *Angew. Chem.* **1999**, *111*, 2045–2048; *Angew. Chem. Int. Ed.* **1999**, *38*, 1920–1923; ; d) R. Paciello, L. Siggel, M. H. J. Kneuper, N. Walker, M. Röper, *J. Mol. Catal. A* **1999**, *143*, 85–97.
- [26] D. Gleich, R. Schmid, W. A. Herrmann, *Organometallics* **1998**, *17*, 4828–4834.
- [27] a) D. Gleich, R. Schmid, W. A. Herrmann, *Organometallics* **1998**, *17*, 2141–2143; b) D. Gleich, W. A. Herrmann, *Organometallics* **1999**, *18*, 4354–4361.
- [28] a) E. J. Baerends, D. E. Ellis, P. Ros, *Chem. Phys.* **1973**, *2*, 41–51; b) C. Fonseca-Guerra, J. G. Snijders, G. te Velde, E. J. Baerends, *Theor. Chem. Acc.* **1998**, *99*, 391–403.
- [29] A. D. Becke, *Phys. Rev. A* **1988**, *38*, 3098–3100.
- [30] J. P. Perdew, *Phys. Rev. B* **1986**, *33*, 8822–8824.
- [31] T. K. Woo, L. Cavallo, T. Ziegler, *Theor. Chem. Acta* **1998**, *100*, 307–313.
- [32] a) M. Clark, R. D. Cramer III, N. van Opdenbosch, *J. Comput. Chem.* **1989**, *10*, 982–1012; b) U. C. Sing, P. A. Kollman, *J. Comput. Chem.* **1986**, *7*, 718–730.
- [33] A. K. Rappé, C. J. Casewit, K. S. Colwell, W. A. Goddard III, W. M. Skiff, *J. Am. Chem. Soc.* **1992**, *114*, 10024–10035.
- [34] P. W. N. M. van Leeuwen *Homogeneous Catalysis*, Kluwer, Dordrecht, **2004**.
- [35] P. W. N. M. van Leeuwen, C. P. Casey, G. T. Whiteker, *Phosphines as Ligands in Rhodium Catalyzed Hydroformylation*, (Eds.: P. W. N. M. van Leeuwen, C. Claver) Kluwer-CMC: Dordrecht, **2000**, pp. 96–106.
- [36] D. Evans, J. A. Osborn, G. Wilkinson, *J. Chem. Soc. (A)* **1968**, 3133–3142.
- [37] F. H. Allen, O. Kennard, *Chem. Des. Autom. News* **1993**, *8*, 31–37.
- [38] S. E. Harris, I. Pascual, A. G. Orpen, *J. Chem. Soc. Dalton Trans.* **2001**, 2996–3009, and references therein.
- [39] P. Haquette, F. Lebideau, S. Dagorne, J. Marrot, G. Jaouen, *Acta Cryst.* **2002**, *C58*, m551 m552.
- [40] E. A. Meyer, R. K. Castellano, F. Diederich, *Angew. Chem.* **2003**, *115*, 1244–1287; *Angew. Chem. Int. Ed.* **2003**, *42*, 1210–1250; , and references therein.
- [41] J. D. Dunitz, A. Gavezotti, *Angew. Chem.* **2005**, *117*, 1796–1819; *Angew. Chem. Int. Ed.* **2005**, *44*, 1766–1787; , and references therein.
- [42] S. Tsuzuki, K. Honda, T. Uchimaru, M. Mikami, K. Tanabe, *J. Am. Chem. Soc.* **2000**, *122*, 3746–3753.
- [43] S. Tsuzuki, K. Honda, T. Uchimaru, M. Mikami, K. Tanabe, *J. Am. Chem. Soc.* **2002**, *124*, 104–112.
- [44] a) M. O. Sinnokrot, E. F. Valeev, C. D. Sherill, *J. Am. Chem. Soc.* **2002**, *124*, 10887–10893; b) M. O. Sinnokrot, C. D. Sherill, *J. Phys. Chem. A* **2004**, *108*, 10200–10207.
- [45] X. Ye, Z. -H. Li, W. Wang, K. Fan, W. Xu, Z. Hua, *Chem. Phys. Lett.* **2004**, *397*, 56–61.
- [46] E. J. Meijer, M. Sprik, *J. Chem. Phys.* **1996**, *105*, 8684–8689.
- [47] a) G. Ujaque, F. Maseras, A. Lledós, *J. Am. Chem. Soc.* **1999**, *121*, 1317–1323; b) J. Vázquez, M. A. Pericás, F. Maseras, A. Lledós, *J. Org. Chem.* **2000**, *65*, 7303–7309; c) E. Daura-Oller, A. M. Segarra, J. M. Poblet, C. Claver, E. Fernández, C. Bo, *J. Org. Chem.* **2004**, *69*, 2669–2680.
- [48] F. Maseras, A. Lledós, *Computational Modeling of Homogeneous Catalysis*, Kluwer, Dordrecht, **2002**.
- [49] H. Krause, B. Ernstberger, H. J. Neusser, *Chem. Phys. Lett.* **1991**, *184*, 411–417.
- [50] J. R. Grover, E. A. Walters, E. T. Hui, *J. Phys. Chem.* **1987**, *91*, 3233–3237.
- [51] In benzene dimer the calculated IE at the CCSD(T) level is 46% lower than that at the MM level. Thus, it is reasonable to assume that the relative energies of pro-S TSs, in which π - π stacking interaction is the major source of energy difference should be lower by such a percentage.
- [52] a) S. Grimme, *J. Comput. Chem.* **2004**, *12*, 1463–1473; b) M. Allen, D. J. Tozer, *J. Chem. Phys.* **2002**, *117*, 11113–11120; c) J. M. Pérez-Jordá, A. D. Becke, *Chem. Phys. Lett.* **1995**, *233*, 134–137; d) S. Kristyán, P. Pulay, *Chem. Phys. Lett.* **1994**, *229*, 175–180.
- [53] T. P. Yoon, E. N. Jacobsen, *Science*, **2003**, *299*, 1691–1693.

Received: May 30, 2005
Published online: November 28, 2005